Additive Manufacturing 74 (2023) 103724

Contents lists available at ScienceDirect

Additive Manufacturing

journal homepage: www.elsevier.com/locate/addma

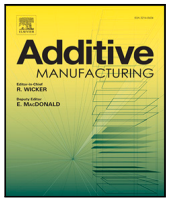

Research paper

Mechanical response of multistable tensegrity-like lattice chains

Claudio Intrigila *, Andrea Micheletti, Nicola A. Nodargi, Paolo Bisegna

Department of Civil Engineering and Computer Science, University of Rome Tor Vergata, Rome, Italy

ARTICLE INFO

Keywords:
Multistable systems
Tensegrity
Lattice metamaterials
Programmable materials
Stereolithography

ABSTRACT

Recent developments in the quality and accuracy of additive manufacturing have drawn particular attention to metamaterials characterised by a multistable response to achieve exceptional mechanical properties. This work focuses on the design, fabrication, testing, and simulation of tensegrity-like lattice chains accomplishing a multistable behaviour. The chains are composed of chiral tensegrity-like units featuring a highly nonlinear bistable response with compression-twisting coupling. Different chains are designed by exploiting the chirality of the units and realised by the inverted stereolithography technique. Their mechanical response is experimentally characterised, demonstrating the attainment of the desired multistable behaviour. A predictive semi-analytical model is derived to reconstruct the multistable energy landscape and force-vs.-displacement curve of the whole chain. The presented chains may constitute a flexible platform for programmable materials, potentially extending to modular chains also based on other types of tensegrity-like units.

1. Introduction

The significant advances in additive manufacturing (AM) techniques of the last years have enabled the fabrication of mechanical metamaterials with an ever-increasing level of accuracy, attracting growing multidisciplinary interest and spanning different technological fields. Mechanical metamaterials have been the subject of numerous studies for their unconventional response to external actions (e.g., [1–8]), which makes them interesting for applications (e.g., [9,10]). A substantial part of the literature focused on the design and analysis of bistable/multistable structures and metamaterials, and it was amply demonstrated that mechanical instabilities can be exploited to store and release energy in order to obtain energy-trapping devices [11,12], stable propagation of solitary waves [13,14], actuators and soft robots [15,16].

The attention is here focused on tensegrity metamaterials which exhibit a wide range of nonlinear mechanical responses and can be suitably tuned up [17–21] (see also [22,23] and references therein). In particular, tensegrity-like structures are considered, which are lattices with the same nodal connectivity of corresponding tensegrities but involve no prestressed elements and thus overcome the relevant manufacturing difficulties [24,25]. For example, in [26], the impact response of additively manufactured tensegrity-like lattices assembled from octahedral units was investigated. It was also demonstrated that microscale tensegrity-like lattices composed of octahedral units have a better failure-resistant behaviour with respect to other types of lattices [27]. Moreover, in [28], a chain of tensegrity-like units inspired by the topological configuration of a six-bar tensegrity was proposed for energy dissipation.

Recent works have progressively addressed the possibility of achieving tensegrity-like metamaterials with bistable behaviour. In [29], a shift from a primary to a secondary stable configuration was shown in the compression response of microscale tensegrity-like lattices based on triangular prismatic tensegrities known as T3 [30], realised by multiphoton lithography. Subsequently, a snapping behaviour was observed in [31] considering a double-T3 unit (dT3) composed of two T3s, additively manufactured using the fused deposition modelling technique. Finally, a clear bistable response was experimentally achieved in [32], resorting to a dT3 unit fabricated via inverted stereolithography technology.

By leveraging the aforementioned results, tensegrity-like units can be envisaged to form multistable chain-like assemblies, whose response can be modelled as a chain of bistable springs by resorting to known analytical methods (see, e.g., [33]). In this way, exploiting the bistability of the additively manufactured tensegrity-like units and circumventing the difficulties of fabrication of traditional tensegrities, such assemblies could emerge as a promising platform for a wide range of functional engineering applications, for instance, robotic mechanisms [34,35], mechanical memory storage devices [36,37], vibration isolators [38] and energy-absorbing architected materials [11,12].

The purpose of this work is to experimentally investigate the mechanical response of tensegrity-like lattice chains composed of bistable dT3 units. The latter, obtained by juxtaposing two T3s with equal

* Corresponding author.
E-mail address: intrigila@ing.uniroma2.it (C. Intrigila).

https://doi.org/10.1016/j.addma.2023.103724
Received 21 April 2023; Received in revised form 11 July 2023; Accepted 2 August 2023
Available online 7 August 2023

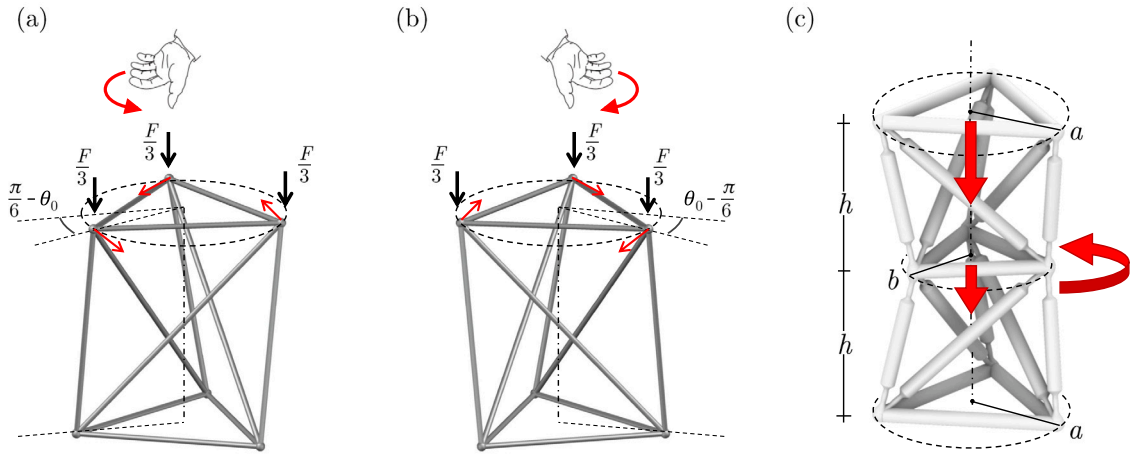

Fig. 1. Tensegrity-like lattice structures: (a) left-handed T3, (b) right-handed T3, and (c) double-T3 unit.

geometry and opposite chirality, are realised monolithically as bistable compliant mechanisms and exhibit a compression-twisting coupling. Exploring the design space offered by the chirality of dT3 units, different chain samples are manufactured via the inverted stereolithography technique and tested. Results of compression tests demonstrate that the fabricated lattices accomplish a multistable response and, by considering different assemblies of the units composing a chain, different compression-twisting responses can be established. Test results are interpreted by a semi-analytical model obtained by fitting the experimental response of one dT3 unit and then by reconstructing the energy landscape and force-vs.-displacement curve of the multistable lattice chains.

The proposed multistable chains exhibit similar kinematics and multistable response compared with those recently obtained through multimodular origami-inspired structures [34–40], mostly based on the Kresling pattern [41]. On the other hand, the possibility to monolithically fabricate multistable tensegrity-like chains with a single material by AM may be competitive with the methods currently employed for the realisation of origami-inspired structures (e.g., [35,36,42]), confirming that tensegrity-like chains may constitute a flexible platform for programmable materials. Finally, the presented design procedure could be adapted to chains based on other types of tensegrity-like units arranged in series or parallel.

This paper is organised as follows. Section 2 introduces the geometrical and mechanical features of the tensegrity-like chains considered in this study, starting from their constituent dT3 unit. Section 3 describes the procedure followed to design the sample geometry and the fabrication steps. Test results are presented in Section 4 for the dT3 and for three assemblies, which differ from each other by the chirality of the individual units. Section 5 is devoted to the elaboration of the semi-analytical model and to the evaluation of its predictive accuracy with respect to the experimental results. A discussion of the experimental and numerical results is given in Section 6. Conclusions are outlined in Section 7.

2. Tensegrity-like lattice chains

The modular structures investigated in this study are assembled from double-T3 units (dT3s), which in turn are composed of two T3 tensegrity-like structures. The latter are obtained from a triangular right frustum by placing bars along all the edges and one diagonal of the lateral faces, with connections at the vertices, so as to obtain a three-fold cyclic-symmetric structure (Fig. 1 (a)). In addition, a frustum base is rotated with respect to the other one about the symmetry axis by a twist angle $\varphi_0 = \pi/6 - \theta_0$, with θ_0 a small overtwist angle, as shown in Fig. 1 (a). In passing, the classical selfstressed tensegrity prism corresponds to the particular case $\theta_0 = 0$. It is well known that a T3 features a compression-twisting coupling: upon compression along the symmetry axis, the two bases undergo a relative screw motion, as shown in Fig. 1 (a), (b). In fact, a T3 is a chiral structure which can be realised in two versions that are mirror images of each other (Fig. 1 (a), (b)). As a notation, a T3 is said left-handed (right-handed) if the diagonal bar connects the bottom-left and the top-right corners (bottom-right and top-left corners) of a lateral face.

The dT3 unit is obtained by the juxtaposition of two T3s with equal geometry and opposite chirality. It follows that, upon compression, the top and bottom bases undergo just a relative vertical translation, while the common middle base translates along and rotates about the symmetry axis (Fig. 1 (c)). The compressive response of an additively manufactured dT3 was studied in [32], experimentally proving that a bistable behaviour with energy trapping can be achieved.

In this work, the mechanical response of chains composed of dT3s is investigated. The motivation comes from the rich compressive–tensile behaviour exhibited by multistable chains composed of bistable springs, as described in [33]. For a qualitative review of such behaviour, let a bistable spring be considered, characterised by the force- and energy-vs.-displacement responses in a hard-device setting shown in Fig. 2 (a) and (b), respectively. The monotonic branches of the force-vs.-displacement curve are identified with Phases 1, 2, and 3. Correspondingly, the energy-vs.-displacement curve is composed of two convex branches (Phases 1 and 3) separated by a concave one (Phase 2). In the following, a bistable spring is defined as 'active' if it is in Phase 2 (i.e., in the unstable branch) and 'inactive' if it is in Phase 1 or 3 (i.e., in a stable branch).

A series assembly of two such bistable springs is characterised by the force- and energy-vs.-displacement responses shown in Fig. 2 (c) and (d), respectively. Let (k,l) denote the assembly configuration, with $k,l = 1,2,3$, the phases of the two springs. Depending on the phases progressively experienced by the individual springs, different deformation paths can be followed by the assembly. A homogeneous deformation path may occur, consisting of the sequence of configurations $(1,1),(2,2),(3,3)$, i.e., the two springs remain in the same phase throughout the test. In fact, the homogeneous case never occurs in practical situations because its energy is higher than in inhomogeneous deformation paths. The latter may consist either of the sequence of configurations $(1,1),(1,2),(1,3),(2,3),(3,3)$, in which the two springs pass through Phase 2 (i.e., they get activated) at different times, or of the isoenergetic alternative sequence $(1,1),(2,1),(3,1),(3,2),(3,3)$, differing for the activation order of the two springs. Which of the two inhomogeneous deformation paths actually takes place is determined by imperfections in fabrication and/or testing conditions.

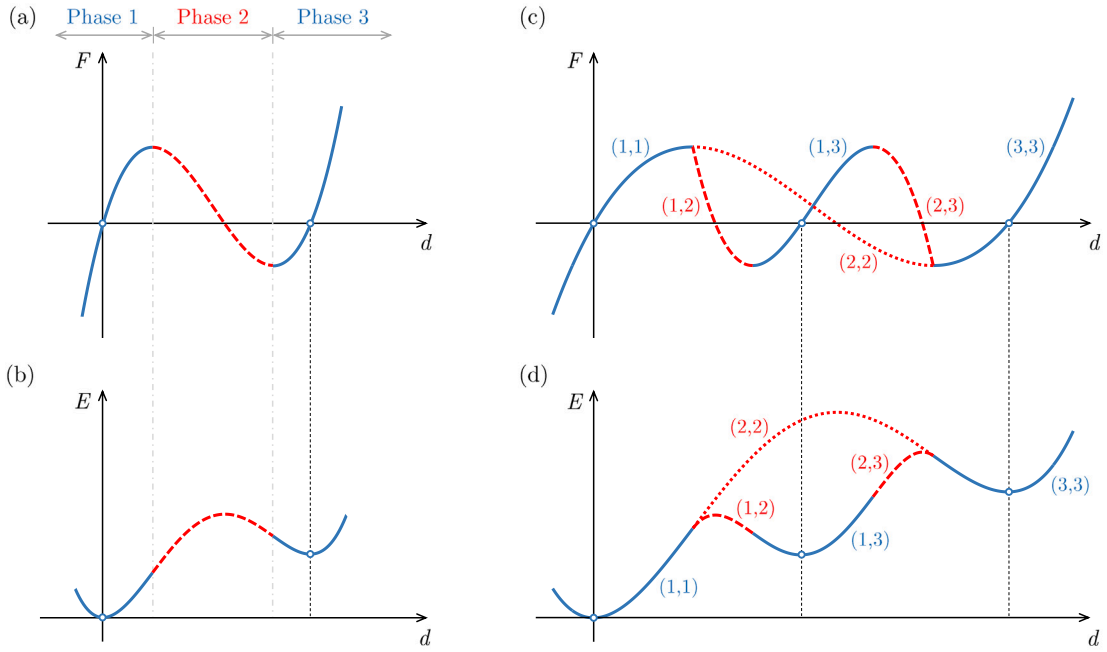

Fig. 2. Force-vs.-displacement curves (top) and corresponding energy (bottom) in a hard-device setting: (a), (b) a bistable spring, the monotonic branches of the force-vs.-displacement curve are identified with Phases 1, 2, and 3; (c), (d) an assembly of two bistable springs in series. The pairs (k, l), with $k, l = 1, 2, 3$, represent the phases of the two springs. Stable branches are shown with blue solid lines, and unstable branches with dashed red lines. The unstable branch $(2, 2)$ is depicted with the dotted red line. (For interpretation of the references to colour in this figure legend, the reader is referred to the web version of this article.)

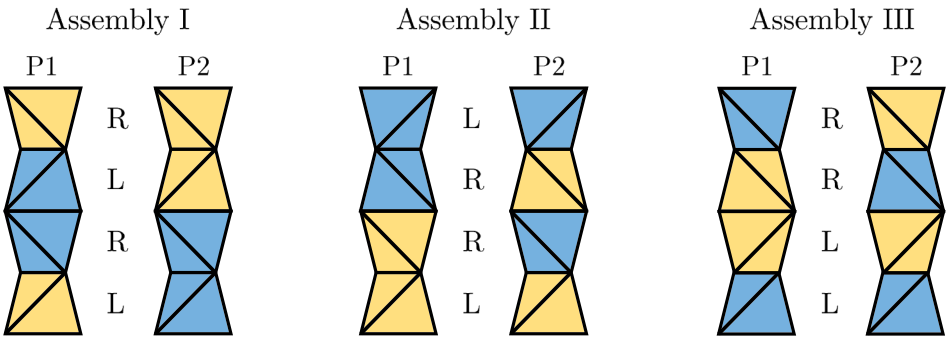

Fig. 3. Multistable tensegrity-like assemblies: scheme of the three different chains (Assembly I, II, III) of two double-T3 tensegrities. Left-handed and right-handed T3s are denoted by the letters L and R, respectively. The yellow and blue shadings indicate the two possible pairings (P1, P2) of the four T3s in each assembly. (For interpretation of the references to colour in this figure legend, the reader is referred to the web version of this article.)

Prompted by such an intriguing mechanical response of chains of bistable springs, chains consisting of two dT3s are investigated in the present study. Recalling that a dT3 is made of two T3s with different chirality, the chains are realised considering all permutations of two left- and two right-handed T3s. Upon identifying mirrored chains, three distinct assemblies are obtained (Assembly I, II, III), shown in Fig. 3.

Since each of the two bistable elements is realised by a dT3 unit, the kinematics of the corresponding chain is richer than the one previously described, obtained with two typical bistable springs. On the one hand, owing to the compression-twisting coupling, each base shared by the T3s may undergo a screw motion. On the other hand, a dT3 unit in a chain does not necessarily pair two adjacent T3s, but it can as well pair two non-adjacent T3s as long as they have opposite chirality. Fig. 3 shows the two possible pairings (P1, P2) of T3s for Assemblies I, II and III. For each pairing, two possible inhomogeneous deformation paths can be distinguished depending on the activation order, i.e., identifying which of the two dT3s passes first through Phase 2. Therefore, four different deformation paths can occur for each assembly, as detailed in Section 6.

3. Design and fabrication

In this section, the design and the fabrication process of the proposed tensegrity-like lattices are described. In particular, the geometries of the designed samples are introduced in Section 3.1, whereas the additive manufacturing process is discussed in Section 3.2.

3.1. Samples geometries

Fig. 1 (c) shows the geometry of the dT3. The bottom and top triangular bases are inscribed in circles with radius $a = 20\,\text{mm}$, while the radius of the circle circumscribing the middle triangular base is $b = 15\,\text{mm}$. Each T3 has overtwist $\theta_0 = 14°$ and height $h = 30\,\text{mm}$. These values were chosen to avoid contact between lattice members, considering the large displacements occurring during compression tests. The lattice members connecting the middle base to the top and bottom bases are subdivided into three segments, i.e., the main body, with constant circular cross-section of diameter $d_\text{b} = 2\,\text{mm}$, and the two end links of length $l_1 = 5\,\text{mm}$. The geometry of the end links was designed with a cylindrical profile of diameter $d_1 = 1\,\text{mm}$ at the centre and a

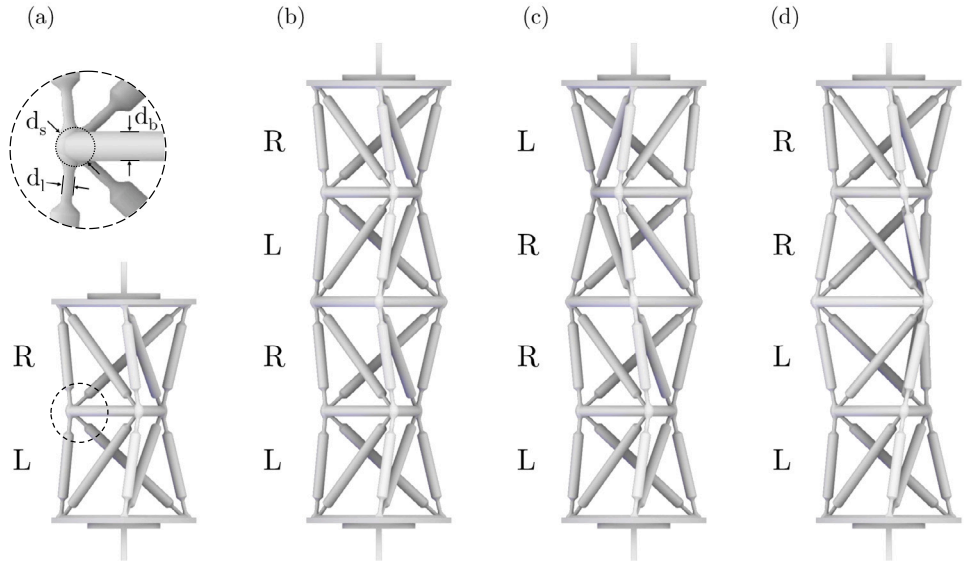

Fig. 4. Geometry of the designed tensegrity-like lattices. (a) 3D geometry of double-T3 unit and detail of the nodal area. Chains of two double-T3 units assembled with different orientation order: (b) Assembly I; (c) Assembly II; (d) Assembly III.

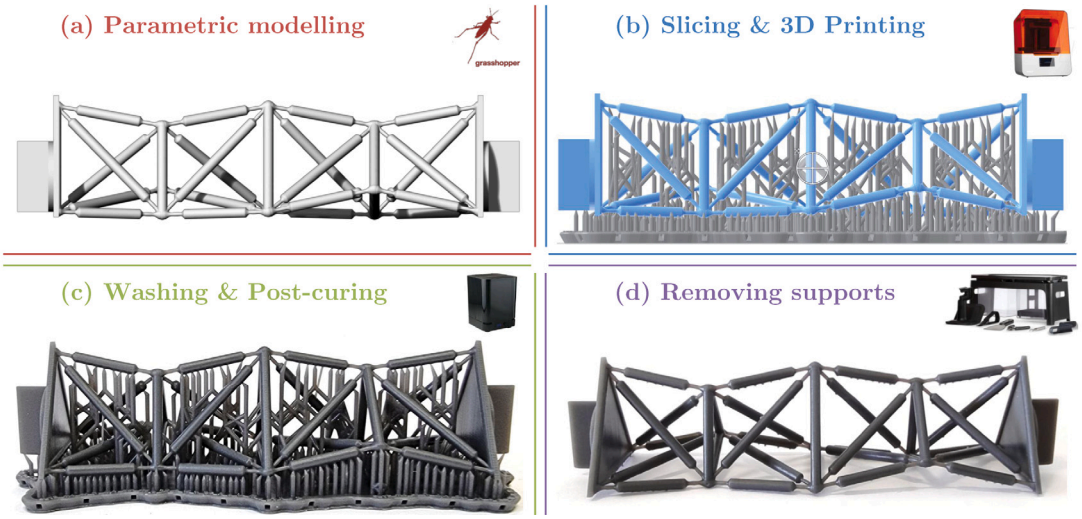

Fig. 5. Fabrication process: (a) parametric geometrical model; (b) preview of the sliced model; (c) printed sample after the washing and post-curing process; (d) printed sample after removing the supports.

smoothly varying diameter to connect to the main body of the member on one side and to the spherical node of diameter $d_n = 3$ mm on the other side, as depicted in Fig. 4 (a). These parameters were set in order to achieve the desired bistable compliant mechanism of the dT3 unit along the line previously traced in [32].

Three distinct chains, corresponding to Assemblies I, II, and III, were assembled from two left-handed and two right-handed T3s arranged in a different order, as shown in Fig. 4 (b), (c), and (d), respectively. Since a sample is subjected to both compression and tension during testing, the outer bases were customarily realised to ensure a proper grip with the clamps of the testing machine and a uniform load transfer to the tensegrity-like chains.

3.2. Samples fabrication

The set of test samples was fabricated through low-force stereolithography (SLA) using the desktop 3D printer Form 3B by Formlabs®, exploiting the PreForm slicing software. The structural material used for the printing was Formlabs Tough 2000 which guarantees a good compromise between large elastic deformations, stiffness, and strength.

The main fabrication steps are summarised as follows (see Fig. 5): (a) generation of the parametric geometrical model, (b) conversion of the geometrical model into an STL file and fabrication of the samples, (c) washing and post-curing, (d) removal of supports.

The geometry of the tensegrity-like unit was generated using Grasshopper®, a plug-in of the CAD Rhinoceros® software. Afterwards, the model was sliced into layers via the PreForm software, obtaining the STL file. In this phase, the set of printing parameters was defined, and the necessary supports were arranged to guarantee stability during the manufacturing and the absence of defects in the resulting sample. In order to optimise the quality of the sample surfaces, the layer thickness resolution was chosen to be 25 μm in the horizontal plane and 50 μm along the vertical direction. Due to the different spatial orientations of the lattice members, the printing orientation does not determine a preferential direction in the mechanical response of the unit (see Section S4 of the Supplementary Information (SI)). Therefore, the printing orientation was chosen to minimise the number of supports.

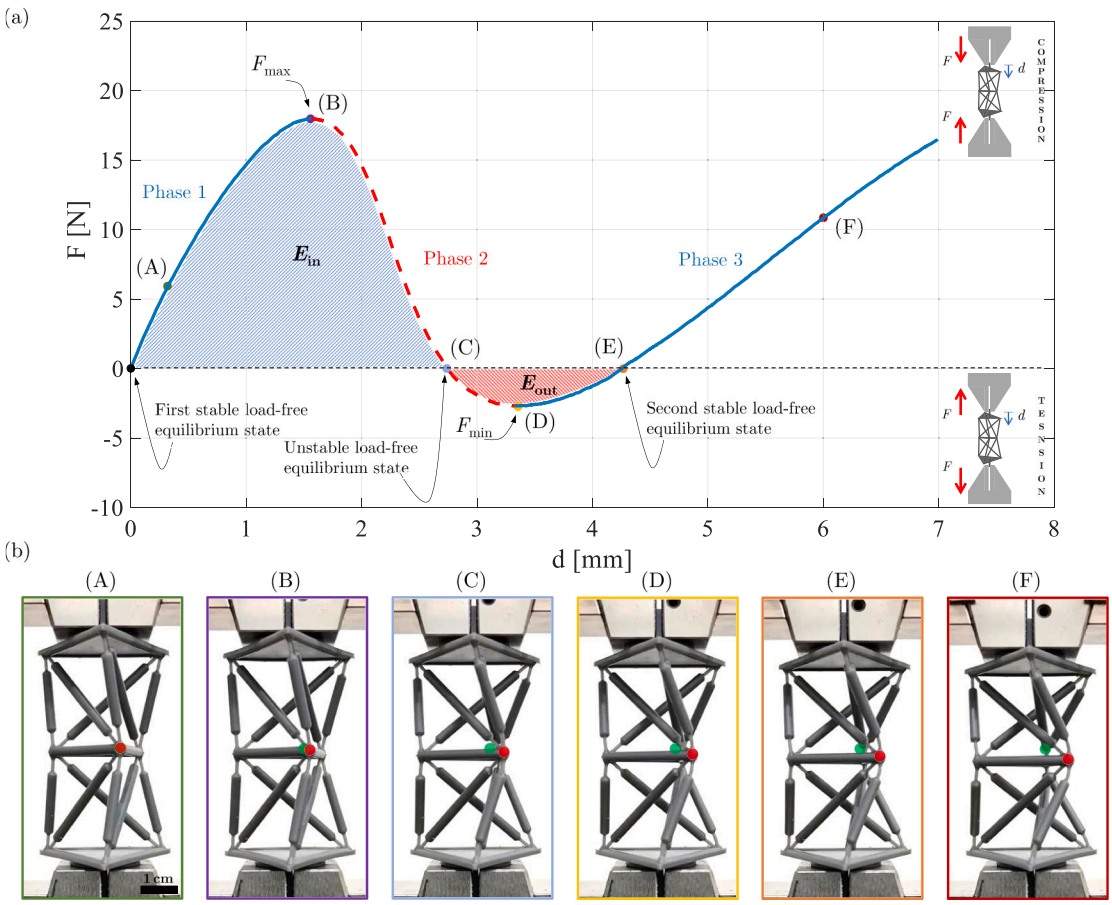

Fig. 6. Results of a compression test on double-T3 tensegrity-like unit: (a) characteristic force-vs.-displacement curve and identification of Phases 1, 2 and 3; (b) selected deformed configurations denoted by (A)–(F) in the force-vs.-displacement curve. The green marker is fixed, whereas the red one follows the unit deformation. (For interpretation of the references to colour in this figure legend, the reader is referred to the web version of this article.)

Once printed, the samples needed to be washed thoroughly to remove uncured resin from the surfaces. That was achieved by immersing the samples in a cleaning chamber filled with tripropylene glycol monomethyl ether for 10 min. Then, the samples were carefully dried using a compressed air machine. The washing and drying steps were preliminary to the post-curing one. The latter is a second polymerisation process, where the sample is placed in a high-temperature oven and exposed again to UV light in all directions. To achieve the highest mechanical properties of the Tough 2000 resin, the temperature was set at 80 °C for 120 min. In this way, it was possible to improve the strength and stiffness of the samples, with a slight reduction in the ultimate deformation [43]. Then, the samples were weighed, and the prime geometric dimensions were measured with a calliper and compared with the CAD model. Finally, the supports were removed.

Moreover, with the aim of investigating the mechanical properties of the parent material (Tough 2000 resin), five type IV tensile specimens were manufactured and tested, as indicated in the ASTM D638-14 [44]. The results of the tests are reported in Section S1 of the SI.

4. Experimental results

The compression tests were performed using an INSTRON 5900R universal testing system under quasi-static displacement control. A 10 kN load cell was used to record the applied load with an acquisition frequency of 20 Hz, while the speed of the mobile crosshead was set at 1 mm/min. A digital camera with a sampling rate of 60 fps at 1080 p resolution was used to document the tests. For statistical and repeatability purposes, three samples for the dT3 unit and for each assembly of the chain were fabricated and tested three times. The tests on the dT3 unit are reported and analysed in Section 4.1. Then, the tests on the tensegrity-like lattice chains are presented and discussed in Section 4.2.

4.1. Double-T3 unit

Fig. 6 (a) shows the characteristic force-vs.-displacement curve (capacity curve) of the dT3 unit under a uniaxial compression test. The deformed configurations relevant to the most significant points in the curve, denoted by (A)–(F), are reported in Fig. 6 (b).

The curve is divided into three monotonic branches corresponding to the phases introduced for a typical bistable spring in Section 2. The first branch (Phase 1, stable) is featured by a nonlinear behaviour and terminates at the force peak (B). The second branch (Phase 2, unstable) is characterised by a negative slope with a high decrease in force, crossing through the unstable load-free equilibrium configuration (C) until the negative limit load is reached (D). In this phase, it is possible to observe a significant geometric transformation characterised by an anticlockwise rotation of the middle base about the vertical axis, besides the imposed vertical displacement. Accordingly, the dT3 is said to be active during Phase 2. As the displacement increases, the equilibrium path enters the third branch (Phase 3, stable), and the force returns to zero when the second stable load-free equilibrium configuration is reached (E). Then, the sign of the force becomes

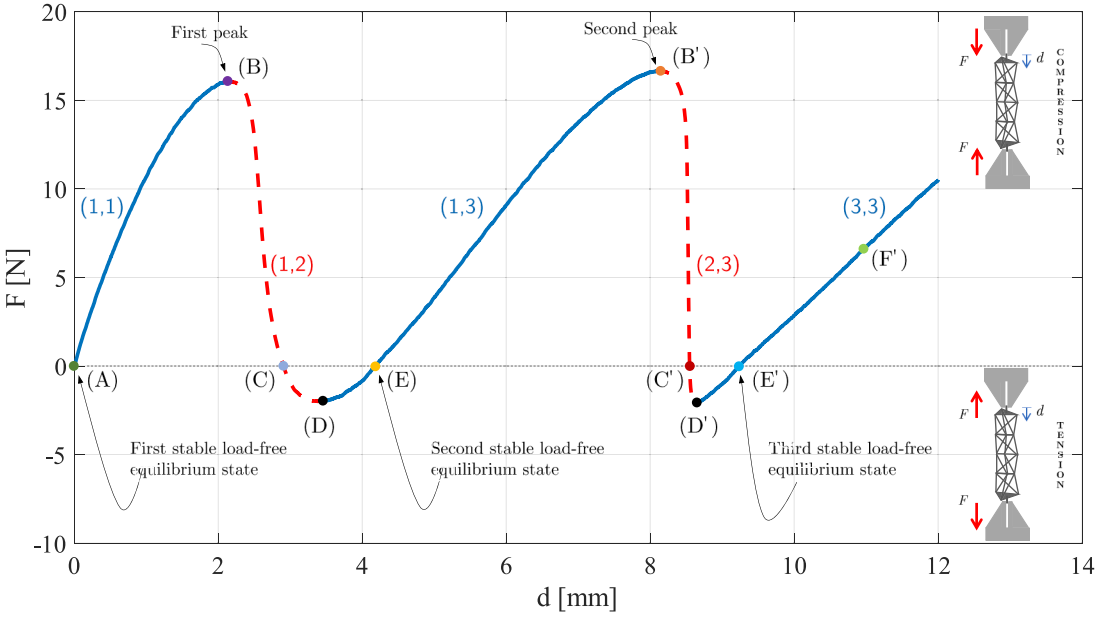

Fig. 7. A characteristic force-vs.-displacement curve of a compression test on a chain of two double-T3s. In the curve, the deformed configurations corresponding to the points denoted by (A)–(F′) are shown in Fig. 8, whereas the pairs (k, l), with $k, l = 1, 2, 3$, represent the phases of the two double-T3s.

positive (compressive) again, with an almost linear trend of the force-vs.-displacement curve. Once a load value close to the peak value (B) is attained, the test is stopped. A video clip of a compression test of the tensegrity-like unit is available in the SI, Video S1.

It is worth noting that, during the test, the deformations are localised in the links that, serving as compliant hinges, permit a large-displacement response and guarantee the achievement of the designed bistable feature of the sample. In addition, the tensegrity-like structure is able to trap energy because the energy stored up to the unstable load-free equilibrium configuration (E_{in}) is larger than the energy released up to the second stable load-free equilibrium configuration (E_{out}).

The force-vs.-displacement curves of all tests (three repetitions for each of the three samples) are reported in Fig. S2 of the SI. The results show good repeatability of the tests with slight deviations from the characteristic response depicted in Fig. 6(a) and no visible damage. Such results are in line with those previously obtained in [32] for samples about twice the size, thus verifying the scalability of the dT3 lattice in regard to its mechanical response.

4.2. Chains of two double-T3 units

In this section, with the aim of investigating the multistable behaviour of tensegrity-like lattice chains, the experimental results on the three SLA-made chains of two dT3s previously described (Assemblies I, II, III) are presented. They exhibit the same characteristic capacity curve under a uniaxial compression test, as reported in Fig. 7.

The response is characterised by three stable load-free configurations accompanied by a significant geometric transformation. The curve can be segmented into two parts, respectively, from point (A) to (E) and from point (E) to (F′), each retracing the behaviour described for a single dT3 in Section 4.1. In fact, the first part corresponds to one dT3 of the chain evolving through Phases 1, 2, and 3, with the other dT3 remaining in Phase 1. Analogously, the second part corresponds to the former dT3 remaining in Phase 3 and the latter one evolving through Phases 1, 2, and 3. However, some differences can be underlined between the two parts. Concerning the limit loads, the second positive peak (B′) is slightly higher than the first one (B). Moreover, the stiffness of the second and third stable branches (DB′ and D′F′) is lower than the first one (AB), while the second unstable branch (B′D′) shows an almost vertical drop of the force down to the negative peak. The interpretation and in-depth discussion of this peculiar response are deferred to Section 5, where a semi-analytical model of the tests is presented.

If, on the one hand, the capacity curve shown in Fig. 7 is representative of all the three proposed assemblies, the kinematics occurring during the test substantially distinguishes them. Selected deformed configurations corresponding to the points (A)–(F′) in the force-vs.-displacement curve of Fig. 7 are reported in Fig. 8 to highlight the differences.

Fig. 8(a) is relevant to Assembly I. The activation of the dT3 that pairs the two external T3s (highlighted with a transparent red hatch) is observed between configurations (B) and (D), with a mechanism similar to the one described for a single dT3 in the previous section. In particular, this mechanism induces a rigid anticlockwise rotation of the other dT3, which pairs the two internal T3s and remains inactive (in Phase 1). In a similar fashion, the activation of the latter dT3 is observed between configurations (B′) and (D′), while the former dT3 remains inactive (in Phase 3). By comparing the deformed configuration (F′) with the undeformed one (A), a significant change in angles between adjacent bars is recognised.

Two alternative deformation paths observed for Assembly II are depicted in Fig. 8(b1) and (b2), highlighting respectively the two possible pairings (P1, P2) of T3s shown in Fig. 3. In Fig. 8(b1), the first active dT3 pairs the two T3s at the bottom. As the imposed vertical displacement increases, the kinematics of the chain is characterised by the alternation of the usual screw motion of the individual dT3s. By contrast, in Fig. 8(b2), the first active dT3 pairs two non-adjacent T3s, i.e., the first and the third one from the bottom of the chain. The mechanism is characterised by an anticlockwise rotation of the second and third bases of the chain, with consequent rigid rotation of the second T3 between them. Once the other dT3 turns active, a mechanism mirroring the previous one occurs. At the end of the tests, the deformed configurations (F′) of Fig. 8(b1) and (b2) are indistinguishable, irrespective of the two distinct deformation paths.

In Fig. 8(c), a deformation path recorded for Assembly III is reported. In particular, the first active dT3 pairs the two internal T3s, featuring the usual screw motion. Once the deformed configuration (B′) is reached, the other dT3, which pairs the external T3s, becomes

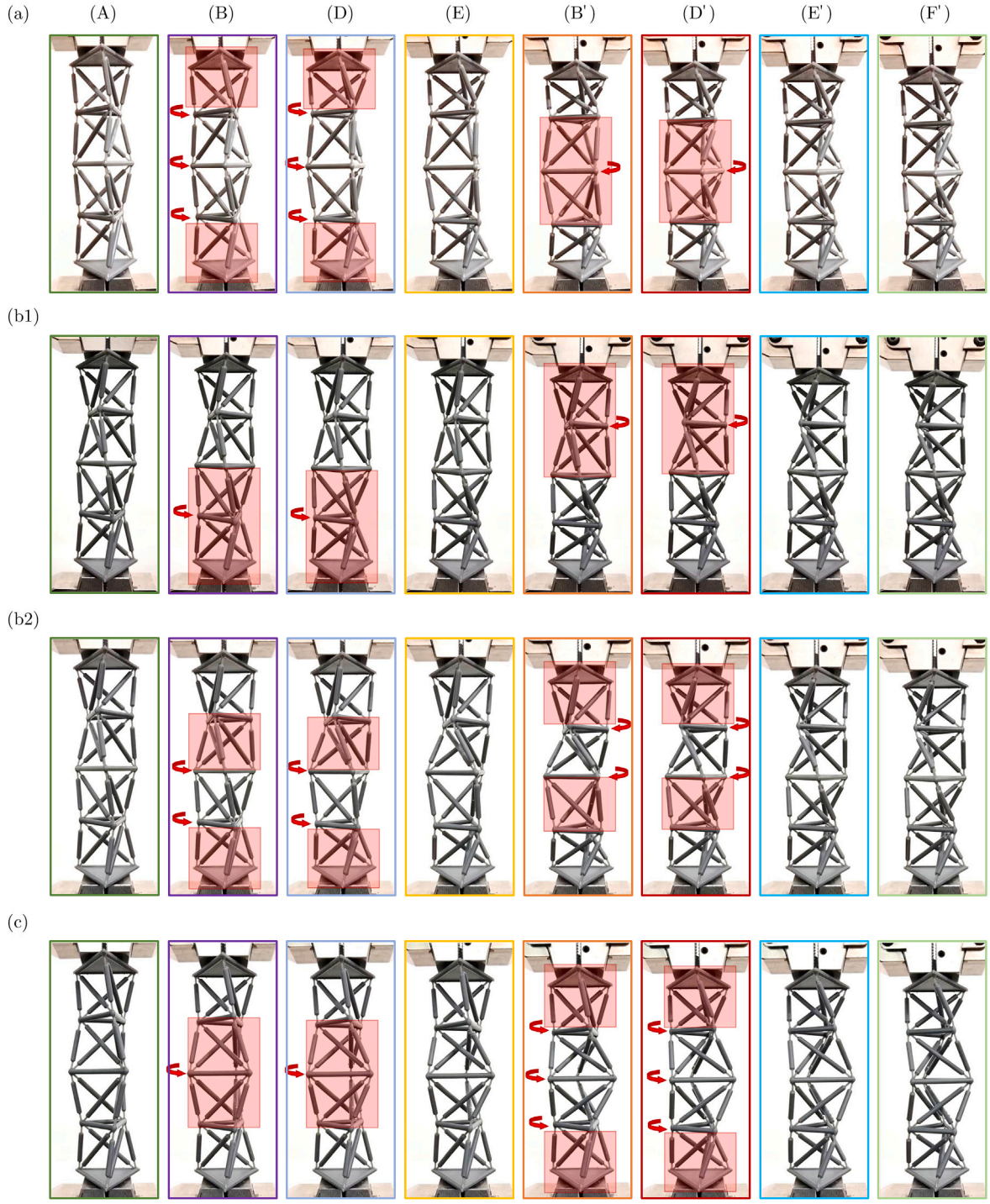

Fig. 8. Results of compression tests. Selected deformed configurations denoted by (A)–(F′) in the force-vs.-displacement curve of Fig. 7: (a) one possible deformation path of Assembly I with pairing P1; (b1, b2) possible deformation paths of Assembly II with pairing P1 and P2, respectively; (c) one possible deformation path of Assembly III with pairing P1. The active double-T3 unit (Phase 2) is highlighted with a transparent red hatch. The red arrows represent the rotation of the intermediate bases along the deformation path. (For interpretation of the references to colour in this figure legend, the reader is referred to the web version of this article.)

active, and its mechanism entails a rigid rotation of the former dT3. In this case, the middle base of the chain is subjected to an anticlockwise rotation in both mechanisms of the two dT3s, leading the assembly to a deformed configuration quite different from the initial one.

Three samples were additively manufactured for each assembly, and three repetitions of the uniaxial compression test were carried out for each sample. The averages of force-vs.-displacement curves of the nine tests for each assembly (I, II, III) are compared in Fig. 9. They are superimposable, up to slight deviations due to unavoidable imperfections and intrinsic variability of the parent material (see Section S1 of the SI).

Results of all the tests on the three samples relevant to Assemblies I, II and III are reported in Fig. S3, S4, and S5 of the SI, respectively. In addition, the movies of the four tests presented in Fig. 8 are included as Video S2, S3, S4 and S5 in the SI, respectively.

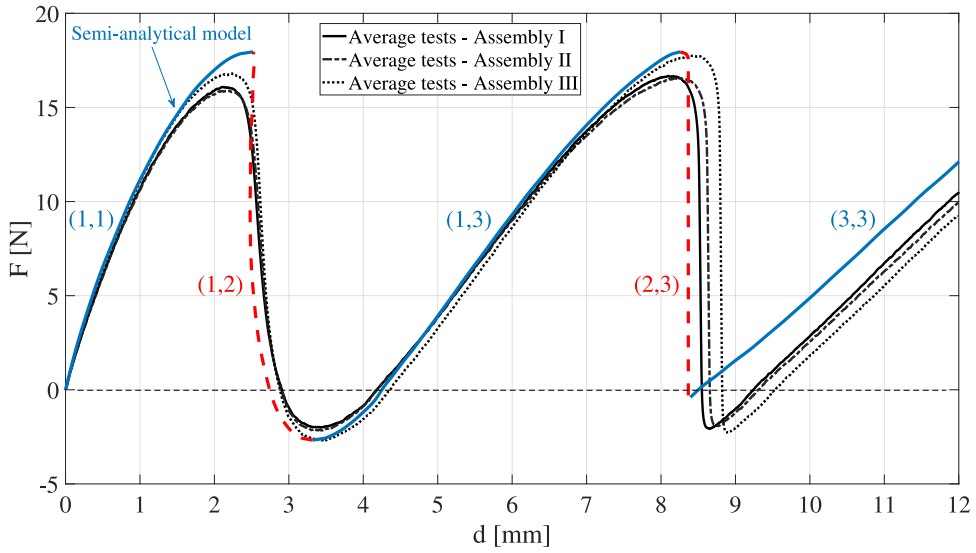

Fig. 9. Experimental uniaxial compressive response of chains of two double-T3s in terms of force-vs.-displacement curves. Average of tests on the three samples relevant to Assembly I, II, and III (black lines). The capacity curve supplied by the semi-analytical model presented in Section 5 is also reported. (For interpretation of the references to colour in this figure legend, the reader is referred to the web version of this article.)

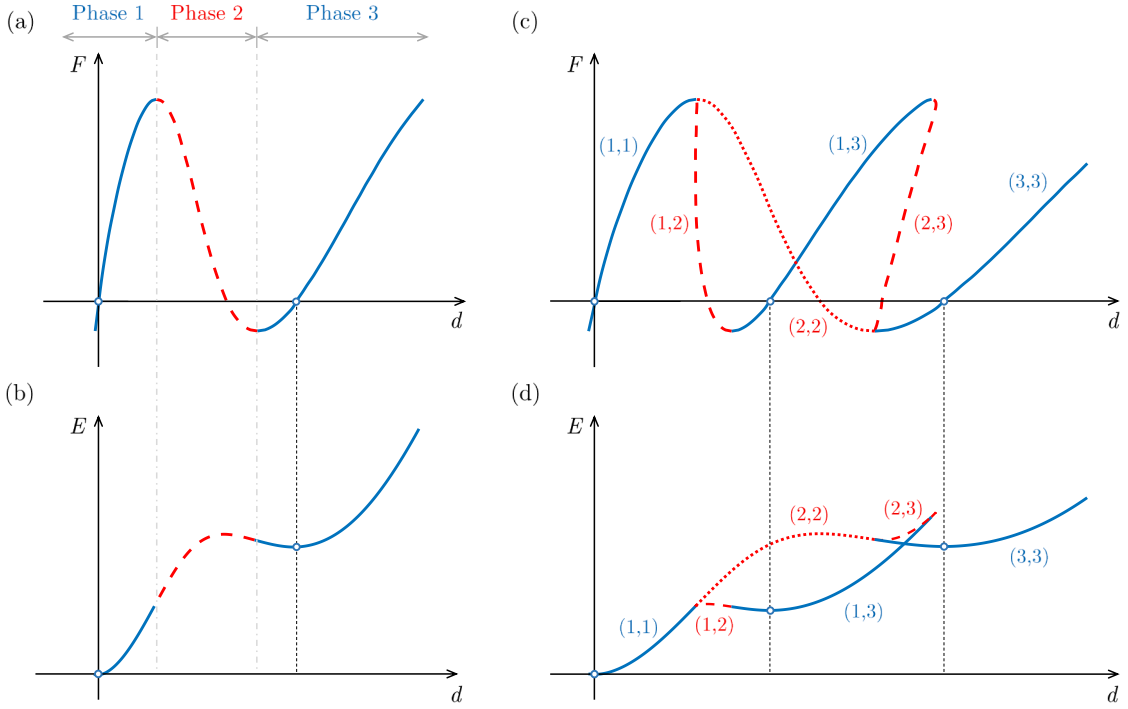

Fig. 10. Semi-analytical response of the double-T3: (a) force-vs.-displacement curve; (b) elastic energy-vs.-displacement curve. Semi-analytical response of the chain of two double-T3s: (c) force-vs.-displacement curve; (d) elastic energy-vs.-displacement curve.

In closing, the present results prove some of the potentialities of the proposed dT3 assemblies in terms of mechanisms and stable states. All the possible responses and deformation paths of the considered chains are illustrated and discussed in Section 6.

5. Semi-analytical model

In this section, a semi-analytical model is proposed for an interpretation of the experimental results. To that end, the average force-vs.-displacement curve experimentally obtained for the dT3 (Fig. 6 (a)) is considered. After removing the effect of the stiffness of the elastic supports (outer plates) [32], a smooth spline interpolation $F(d)$ is derived for the resulting capacity curve, as detailed in Section S3 of the SI.

Fig. 10 (a) and (b) show the interpolating function $F(d)$ and the corresponding energy $E(d)$, respectively. The interpolating function $F(d)$ is segmented into its three monotonic branches $F_i(d)$, with $i = 1, 2, 3$, corresponding to the three phases of a dT3. The inverse functions $d_i(F)$, $F \in (F_{\min}, F_{\max})$, $i = 1, 2, 3$, with $F_{\min}$ and $F_{\max}$ as the negative and positive peak values respectively, are used to reconstruct the response of the chains. For each value of $F \in (F_{\min}, F_{\max})$ the displacement value on each branch (k, l) is thus obtained as $d_{(k,l)} = d_k + d_l$.

Fig. 10 (c) and (d) respectively show the resulting force and energy-vs.-displacement curves of the chain. From Fig. 10 (c), it can be noticed

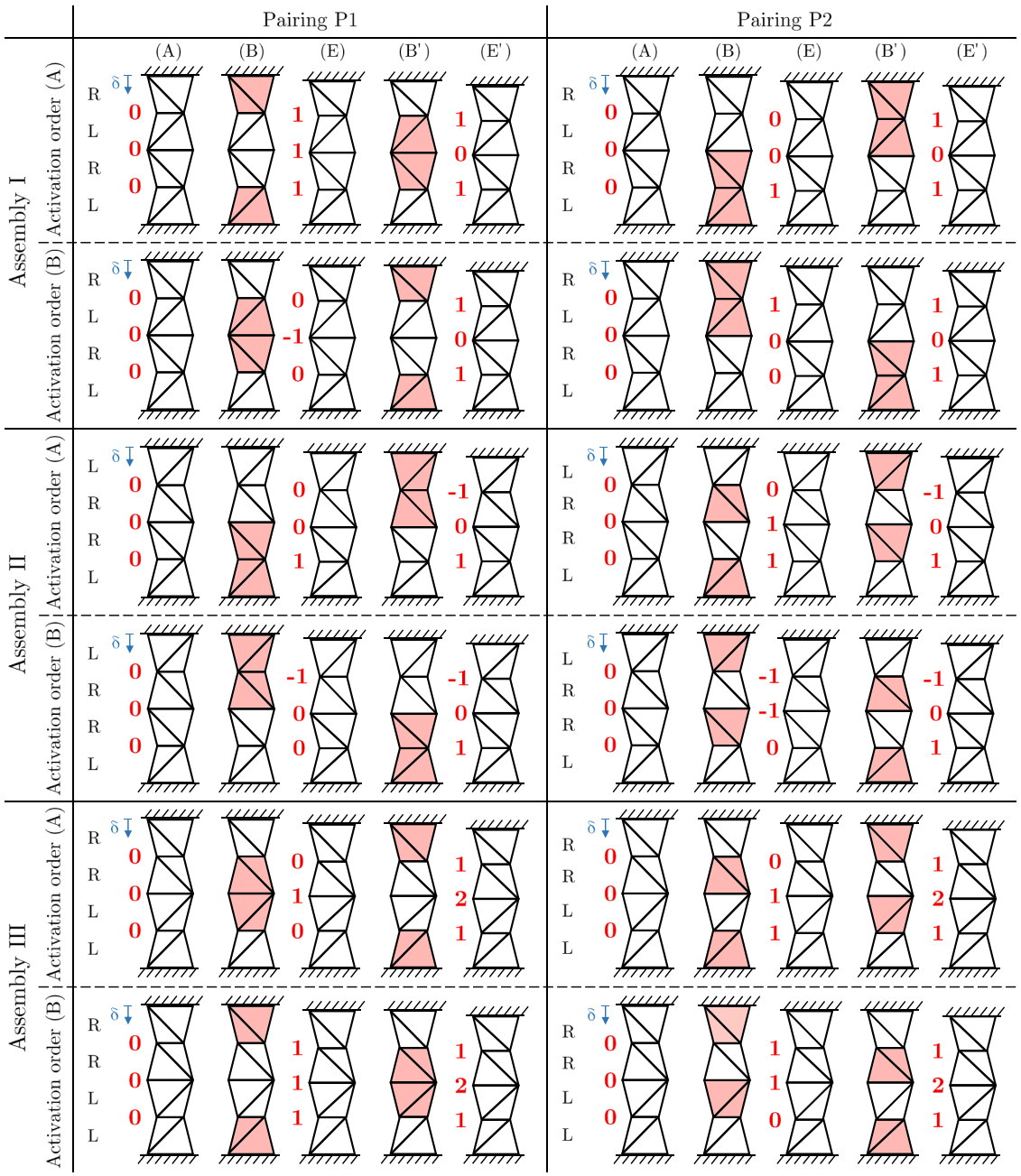

Fig. 11. Schematic illustration of the four possible deformation paths for Assembly I, II, III. For each assembly, the three stable load-free configurations denoted by (A), (E), (E′) in the force-vs.-displacement curve of Fig. 7 are outlined, highlighting with a transparent red hatch the active double-T3 unit ((B), (B′)). The integers denote the rotations of the three triangular bases in unit of $\bar{\theta}$. (For interpretation of the references to colour in this figure legend, the reader is referred to the web version of this article.)

that the first unstable branch exhibits an approximately vertical drop of the force down to the negative peak, whereas a marked snap-back characterises the second unstable branch, as also evidenced by the cusps of the energy curve in Fig. 10 (d). By recalling that the two unstable branches respectively correspond to configurations $(1,2)$ and $(2,3)$ of the chain, that is explained because $d_1'(F) + d_2'(F)$ is mostly positive, whereas $d_2'(F) + d_3'(F)$ is mostly negative (here a prime denotes differentiation with respect to F).

Fig. 9 compares the averages of the experimental force-vs.-displacement curves obtained for the three samples of Assemblies I, II, and III with the semi-analytical curve. For consistency with the experimental tests carried out under displacement control, in the semi-analytical curve, the influence of the stiffness of the elastic supports has been added back, and the predicted snap-back response has been replaced by a vertical drop of the force. A good agreement of the semi-analytical curve with the experimental ones is observed, in particular for the first three branches $(1,1)$, $(1,2)$, and $(1,3)$. It is also highlighted that while the semi-analytical curve is characterised by positive peaks corresponding to the same load value, in the experimental curves, the load value at the first positive peak is slightly lower than the one at the second positive peak. Those small differences might be due to the simplified estimation of the stiffness of the elastic supports, the increasing influence of geometric nonlinearities as the test proceeds, and the unavoidable imperfections of the tested samples.

6. Discussion

The performed experiments show that the response of tensegrity-like lattice chains of two dT3s in terms of the force-vs.-displacement curve is not affected by either the assembly of T3s or the deformation

path. In fact, the four possible inhomogeneous deformation paths for each assembly (determined by the two possible pairings and the two possible activation orders (see Section 2)) influence only the kinematics of the chain. A complete account of the possible deformation paths is depicted in Fig. 11. As an example, for Assembly II, it can be noticed that the schematic illustrations relevant to Pairings P1 and P2 and to the Activation order (A) correspond to the deformation paths experimentally observed in Fig. 8 (b1) and (b2), respectively.

The resulting pattern of possible bistable mechanisms for the proposed assemblies suggests their potential use as mechanical memory storage devices. In particular, by denoting with $\overline{\theta}$ the change of twist occurring in each T3 when passing from one stable configuration to the other one, the integers shown in Fig. 11 correspond to the absolute rotations of the three triangular bases expressed as multiples of $\overline{\theta}$ (the measured value of $\overline{\theta}$ is equal to about 25°).

With the aim of further assessing the multistable response of tensegrity-like lattice chains, a triple-dT3 assembly was fabricated and tested. In particular, the chain was realised with the same design and fabrication process described in Section 3, assembling three left- and three right-handed T3s. The characteristic force-vs.-displacement curve of the triple dT3 and a movie of a test are reported in Fig. S7 and Video S6 of the SI, respectively. As expected, the response is characterised by four stable load-free equilibrium configurations and a sequence of mechanisms similar to the one previously described for chains of two dT3s, thus proving the possibility and effectiveness of manufacturing complex multistable tensegrity-like lattice chains using a fairly accessible low-force stereolithography technology.

The rich mechanical response of the proposed assemblies highlights how these types of lattices constitute a flexible platform for programmable materials. On the one hand, by considering a chain composed of N dT3s, there is a number m of assemblies equal to:

$$m = \frac{1}{2}\frac{(2N)!}{N!^2}, \tag{1}$$

where the half factor results from identifying the mirrored chains. For each assembly, there are $N!$ possible pairings of T3s to form dT3s, $N!$ different activation orders, and $N+1$ stable load-free equilibrium configurations for each deformation path.

On the other hand, driving the pairing of T3s and the activation order of dT3s, i.e., the deformation path that takes place, can be made possible by tuning the mechanical response of the constituting units through a modification of a few geometric parameters as investigated in [32]. As an example, it would be possible to realise dT3 units with different stiffness by choosing different values of the overtwist θ_0, the height h, or the link diameter d_l to induce a specific activation order. Alternatively, the units could be equipped with low-force actuators, e.g., made of the magnetically responsive material presented in [34], to achieve untethered and local/distributed actuation with controllable speed and allow for the independent activation of any unit.

Finally, a computational approach based on beam finite element formulations might be helpful to obtain an alternative numerical model to the semi-analytical one. That would be instrumental for predicting the behaviour of the chains and guiding the optimisation process of the units to reach customised responses. As a result, programmable devices might be obtained, acting as reconfigurable articulations of a modular soft robot [35], or as mechanical memory bit operators and basic logic gates [34,36].

7. Conclusions

The mechanical response of tensegrity-like lattice chains composed of chiral bistable tensegrity-like units has been investigated, proving their multistable behaviour. The considered unit is obtained by juxtaposing two triangular prismatic tensegrity-like structures with chiral geometry and compression-twisting coupling, realised as bistable compliant mechanisms. Different chains have been additively manufactured via the inverted stereolithography technique by considering different assemblies and chiralities of the units. For the experimental characterisation of the response of such chains, samples were loaded in compression and tension during displacement-control tests. Results showed the expected multistable response of the chains, with high repeatability of the tests and a large collection of possible mechanisms, confirming that these types of lattices constitute a flexible platform for programmable materials. A semi-analytical model has been proposed to reconstruct the energy landscape and force-vs.-displacement curve of the multistable lattice chains, giving an in-depth interpretation of the peculiar response of such tensegrity-like chains.

When comparing the present results to previous similar studies on multimodular origami-inspired structures, analogous kinematics featured by the multistable response can be achieved with the proposed tensegrity-like lattice chains. Hence, the chains could be used for the same potential applications, such as reconfigurable robotic articulations or as mechanical memory storage devices and basic logic gates. Moreover, the advantage of easier manufacture might make tensegrity-like chains preferable to origami-inspired structures. By avoiding the need of pin joints or pretension cables, the proposed procedure can be extended to modular additively manufactured chains based on other types of tensegrity-like units.

CRediT authorship contribution statement

Claudio Intrigila: Conceptualization, Methodology, Formal analysis, Investigation, Writing – original draft, Visualization. **Andrea Micheletti:** Conceptualization, Methodology, Formal analysis, Writing – original draft, Visualization. **Nicola A. Nodargi:** Conceptualization, Methodology, Formal analysis, Writing – review & editing. **Paolo Bisegna:** Conceptualization, Methodology, Formal analysis, Writing – review & editing, Funding acquisition.

Declaration of competing interest

The authors declare that they have no known competing financial interests or personal relationships that could have appeared to influence the work reported in this paper.

Data availability

Data will be made available on request.

Acknowledgments

The presented work was supported by the Italian Minister of University and Research through the project “A bridge to the future: computational methods, innovative applications, experimental validations of new materials and technologies” (No. 2017L7X3CS) within the PRIN 2017 program and by University of Rome Tor Vergata, Italy through the project “OPTYMA” (CUP E83C22002290005) within the “Ricerca Scientifica di Ateneo 2021” program.

Appendix A. Supplementary data

Supplementary material related to this article can be found online at https://doi.org/10.1016/j.addma.2023.103724.

References

[1] V.S. Deshpande, M.F. Ashby, N.A. Fleck, Foam topology: bending versus stretching dominated architectures, Acta Mater. 49 (6) (2001) 1035–1040, http://dx.doi.org/10.1016/S1359-6454(00)00379-7.

[2] A.G. Evans, J.W. Hutchinson, N.A. Fleck, M.F. Ashby, H.N.G. Wadley, The topological design of multifunctional cellular metals, Prog. Mater. Sci. 46 (3–4) (2001) 309–327, http://dx.doi.org/10.1016/S0079-6425(00)00016-5.

[3] N.A. Fleck, V.S. Deshpande, M.F. Ashby, Micro-architectured materials: past, present and future, Proc. Math. Phys. Eng. Sci. 466 (2121) (2010) 2495–2516, http://dx.doi.org/10.1098/rspa.2010.0215.

[4] M.H. Yousuf, W. Abuzaid, M. Alkhader, 4D printed auxetic structures with tunable mechanical properties, Addit. Manuf. 35 (2020) 101364, http://dx.doi.org/10.1016/j.addma.2020.101364.

[5] N.A. Nodargi, P. Bisegna, The saint-venant problem for general anisotropic piezoelectric cylinders with applications to smart metamaterials design, Appl. Math. Model. 93 (2021) 831–851, http://dx.doi.org/10.1016/j.apm.2021.01.003.

[6] C. Intrigila, N.A. Nodargi, P. Bisegna, The compressive response of additively-manufactured hollow truss lattices: an experimental investigation, Int. J. Adv. Manuf. Technol. 120 (2022) 3529–3541, http://dx.doi.org/10.1007/s00170-022-08716-0.

[7] K. Lussenburg, A. Sakes, P. Breedveld, Design of non-assembly mechanisms: A state-of-the-art review, Addit. Manuf. 39 (2021) 101846, http://dx.doi.org/10.1016/j.addma.2021.101846.

[8] P. Bisegna, N.A. Intrigila, C. Nodargi, Design of piezoelectric lattice metamaterials, in: ECCOMAS Congress 2022-8th European Congress on Computational Methods in Applied Sciences and Engineering, 2022, http://dx.doi.org/10.23967/eccomas.2022.082.

[9] W. Wu, W. Hu, G. Qian, H. Liao, X. Xu, F. Berto, Mechanical design and multifunctional applications of chiral mechanical metamaterials: A review, Mater. Des. 180 (2019) 107950, http://dx.doi.org/10.1016/j.matdes.2019.107950.

[10] M. Askari, D.A. Hutchins, P.J. Thomas, L. Astolfi, R.L. Watson, M. Abdi, M. Ricci, S. Laureti, L. Nie, S. Freear, R. Wildman, C. Tuck, M. Clarke, E. Woods, A.T. Clare, Additive manufacturing of metamaterials: A review, Addit. Manuf. 36 (2020) 101562, http://dx.doi.org/10.1016/j.addma.2020.101562.

[11] S. Shan, S.H. Kang, J.R. Raney, P. Wang, L. Fang, F. Candido, J.A. Lewis, K. Bertoldi, Multistable architected materials for trapping elastic strain energy, Adv. Mater. 27 (29) (2015) 4296–4301, http://dx.doi.org/10.1002/adma.201501708.

[12] Y. Chen, L. Jin, Reusable energy-absorbing architected materials harnessing snapping-back buckling of wide hyperelastic columns, Adv. Funct. Mater. 31 (31) (2021) 2102113, http://dx.doi.org/10.1002/adfm.202102113.

[13] J.R. Raney, N. Nadkarni, C. Daraio, D.M. Kochmann, J.A. Lewis, K. Bertoldi, Stable propagation of mechanical signals in soft media using stored elastic energy, Proc. Natl. Acad. Sci. 113 (35) (2016) 9722–9727, http://dx.doi.org/10.1073/pnas.1604838113.

[14] S. Katz, S. Givli, Solitary waves in a bistable lattice, Extreme Mech. Lett. 22 (2018) 106–111, http://dx.doi.org/10.1016/j.eml.2018.06.003.

[15] Y. Chi, Y. Li, Y. Zhao, Y. Hong, Y. Tang, J. Yin, Bistable and multistable actuators for soft robots: Structures, materials, and functionalities, Adv. Mater. 34 (19) (2022) 2110384, http://dx.doi.org/10.1002/adma.202110384.

[16] A. Pal, V. Restrepo, D. Goswami, R.V. Martinez, Exploiting mechanical instabilities in soft robotics: control, sensing, and actuation, Adv. Mater. 33 (19) (2021) 2006939, http://dx.doi.org/10.1002/adma.202006939.

[17] F. Fraternali, L. Senatore, C. Daraio, Solitary waves on tensegrity lattices, J. Mech. Phys. Solids 60 (6) (2012) 1137–1144, http://dx.doi.org/10.1016/j.jmps.2012.02.007.

[18] F. Fraternali, G. Carpentieri, A. Amendola, R.E. Skelton, V.F. Nesterenko, Multiscale tunability of solitary wave dynamics in tensegrity metamaterials, Appl. Phys. Lett. 105 (20) (2014) 201903, http://dx.doi.org/10.1063/1.4902071.

[19] A. Micheletti, G. Ruscica, F. Fraternali, On the compact wave dynamics of tensegrity beams in multiple dimensions, Nonlinear Dynam. 98 (4) (2019) 2737–2753, http://dx.doi.org/10.1007/s11071-019-04986-8.

[20] D.S. Shah, J.W. Booth, R.L. Baines, K. Wang, M. Vespignani, K. Bekris, R. Kramer-Bottiglio, Tensegrity robotics, Soft Robot. 9 (4) (2022) 639–656, http://dx.doi.org/10.1089/soro.2020.0170.

[21] S. Watanabe, Y. Ikemoto, J. Shintake, Modeling and characterization of tensegrity structures integrating dielectric elastomer actuators, Adv. Eng. Mater. 25 (2022) 2201471, http://dx.doi.org/10.1002/adem.202201471.

[22] A. Micheletti, P. Podio-Guidugli, Seventy years of tensegrities (and counting), Arch. Appl. Mech. 92 (9) (2022) 2525–2548, http://dx.doi.org/10.1007/s00419-022-02192-4.

[23] Y. Liu, Q. Bi, X. Yue, J. Wu, B. Yang, Y. Li, A review on tensegrity structures-based robots, Mech. Mach. Theory 168 (2022) 104571, http://dx.doi.org/10.1016/j.mechmachtheory.2021.104571.

[24] A. Amendola, E. Hernández-Nava, R. Goodall, I. Todd, R.E. Skelton, F. Fraternali, On the additive manufacturing, post-tensioning and testing of bi-material tensegrity structures, Compos. Struct. 131 (2015) 66–71, http://dx.doi.org/10.1016/j.compstruct.2015.04.038.

[25] H. Lee, Y. Jang, J.K. Choe, S. Lee, H. Song, J.P. Lee, N. Lone, J. Kim, 3D-printed programmable tensegrity for soft robotics, Science Robotics 5 (45) (2020) eaay9024, http://dx.doi.org/10.1126/scirobotics.aay9024.

[26] K. Pajunen, P. Johanns, R.K. Pal, J.J. Rimoli, C. Daraio, Design and impact response of 3d-printable tensegrity-inspired structures, Mater. Des. 182 (2019) 107966, http://dx.doi.org/10.1016/j.matdes.2019.107966.

[27] J. Bauer, J.A. Kraus, C. Crook, J.J. Rimoli, L. Valdevit, Tensegrity metamaterials: toward failure-resistant engineering systems through delocalized deformation, Adv. Mater. 33 (10) (2021) 2005647, http://dx.doi.org/10.1002/adma.202005647.

[28] H. Zeng, R. Mu, K. Huo, H. Zhao, K. Wang, A. Wang, A novel 3d-printable tensegrity-inspired metamaterial enabling dynamic attenuation, Int. J. Mech. Mater. Des. (2023) 1–19, http://dx.doi.org/10.1007/s10999-023-09656-7.

[29] Z. Vangelatos, A. Micheletti, C.P. Grigoropoulos, F. Fraternali, Design and testing of bistable lattices with tensegrity architecture and nanoscale features fabricated by multiphoton lithography, Nanomaterials 10 (4) (2020) 652, http://dx.doi.org/10.3390/nano10040652.

[30] I.J. Oppenheim, W.O. Williams, Tensegrity prisms as adaptive structures, in: ASME International Mechanical Engineering Congress and Exposition: Adaptive Structures and Material Systems, 1997, pp. 113–120, http://dx.doi.org/10.1115/IMECE1997-0184.

[31] A. Micheletti, C. Intrigila, N.A. Nodargi, E. Artioli, F. Fraternali, P. Bisegna, Modeling and design of periodic lattices with tensegrity architecture and highly nonlinear response, in: M. Papadrakakis, M. Fragiadakis (Eds.), COMPDYN 2021: 8th ECCOMAS Thematic Conference on Computational Methods in Structural Dynamics and Earthquake Engineering, 2021, pp. 1848–1855, http://dx.doi.org/10.7712/120121.8605.19232.

[32] C. Intrigila, A. Micheletti, N.A. Nodargi, E. Artioli, P. Bisegna, Fabrication and experimental characterization of a bistable tensegrity-like unit for lattice metamaterials, Addit. Manuf. 57 (2022) 102946, http://dx.doi.org/10.1016/j.addma.2022.102946.

[33] G. Puglisi, L. Truskinovsky, Mechanics of a discrete chain with bi-stable elements, J. Mech. Phys. Solids 48 (1) (2000) 1–27, http://dx.doi.org/10.1016/S0022-5096(99)00006-X.

[34] L.S. Novelino, Q. Ze, S. W, G.H. Paulino, R. Zhao, Untethered control of functional origami microrobots with distributed actuation, Proc. Natl. Acad. Sci. 117 (39) (2020) 24096–24101, http://dx.doi.org/10.1073/pnas.2013292117.

[35] J. Kaufmann, P. Bhovad, S. Li, Harnessing the multistability of kresling origami for reconfigurable articulation in soft robotic arms, Soft Robot. 9 (2) (2022) 212–223, http://dx.doi.org/10.1089/soro.2020.0075.

[36] H. Yasuda, T. Tachi, M. Lee, J. Yang, Origami-based tunable truss structures for non-volatile mechanical memory operation, Nature Commun. 8 (1) (2017) 1–7, http://dx.doi.org/10.1038/s41467-017-00670-w.

[37] B. Treml, A. Gillman, P. Buskohl, R. Vaia, Origami mechanologic, Proc. Natl. Acad. Sci. 115 (27) (2018) 6916–6921, http://dx.doi.org/10.1073/pnas.1805122115.

[38] S. Ishida, K. Suzuki, H. Shimosaka, Design and experimental analysis of origami-inspired vibration isolator with quasi-zero-stiffness characteristic, J. Vib. Acoust. 139 (5) (2017) http://dx.doi.org/10.1115/1.4036465.

[39] Z. Li, N. Kidambi, L. Wang, K.-W. Wang, Uncovering rotational multifunctionalities of coupled kresling modular structures, Extreme Mech. Lett. 39 (2020) 100795, http://dx.doi.org/10.1016/j.eml.2020.100795.

[40] L. Lu, X. Dang, F. Feng, P. Lv, H. Duan, Conical kresling origami and its applications to curvature and energy programming, Proc. R. Soc. Lond. Ser. A Math. Phys. Eng. Sci. 477 (2257) (2022) 20210712, http://dx.doi.org/10.1098/rspa.2021.0712.

[41] B. Kresling, The fifth fold: Complex symmetries in kresling–origami patterns, Symmetry: Cult. Sci. 31 (2020) 403–416, http://dx.doi.org/10.26830/symmetry_2020_4_403.

[42] S. Khazaaleh, R. Masana, M.F. Daqaq, Combining advanced 3d printing technologies with origami principles: A new paradigm for the design of functional, durable, and scalable springs, Composites B 236 (2022) 109811, http://dx.doi.org/10.1016/j.compositesb.2022.109811.

[43] C. Riccio, M. Civera, O. Grimaldo Ruiz, P. Pedullà, M. Rodriguez Reinoso, G. Tommasi, M. Vollaro, V. Burgio, C. Surace, Effects of curing on photosensitive resins in sla additive manufacturing, Appl. Mech. 2 (4) (2021) 942–955, http://dx.doi.org/10.3390/applmech2040055.

[44] Standard Test Method for Tensile Properties of Plastics, ASTM D638-14, ASTM International, West Conshohocken, PA, 2014, http://dx.doi.org/10.1520/D0638-14.